Curing kinetics and shape-memory behavior of an intrinsically toughened epoxy resin system

Mengjin Fan · Xiangyuan Li · Junying Zhang · Jue Cheng

Abstract   A diglycidylether of propoxylated bisphenol-A with two oxypropylene units (DGEBAPO-2) was prepared, and the structure was characterized by FTIR, ^{1}H NMR, and ESI–MS, and a flexible curing agent 2-methyl-1,5-pentanediamine (MPDA) was used to obtain an intrinsically toughened network for potential shape-memory application. The curing kinetics of DGEBAPO-2/MPDA was systematically investigated by using both non-isothermal and isothermal DSC methods; in addition, the dynamic mechanical property, mechanical property, and shape-memory property were investigated by DMA, tensile experiment, and quantitative shape-memory evaluation method. The results showed that Šesták-Berggren model and Kamal model were able to well describe the non-isothermal curing reaction rate and isothermal curing reaction rate, respectively. Tensile test at 49 °C indicated that the cured DGEBAPO-2/MPDA combined a relatively large elongation at break of 95.53 ± 2.27 % with a relatively large tensile stress of 6.33 ± 0.11 MPa. Quantitative shape-memory evaluation revealed good shape-memory properties of cured DGEBAPO-2/MPDA with shape fixity of 98.88 ± 0.04 % and shape recovery of 96.67 ± 6.91 %.

Keywords   Toughened epoxy resin · DSC · Non-isothermal curing · Isothermal curing · Shape-memory property

M. Fan · X. Li · J. Zhang (✉) · J. Cheng (✉)
Key Laboratory of Carbon Fiber and Functional Polymers (Beijing University of Chemical Technology), Ministry of Education, Beijing 100029, People's Republic of China
e-mail: zjybuct@gmail.com
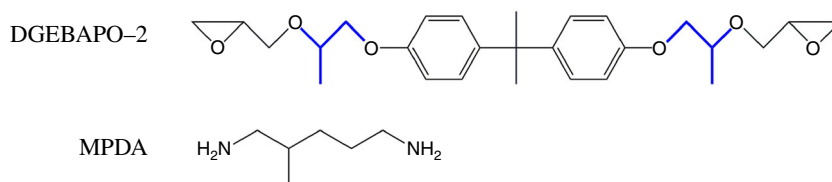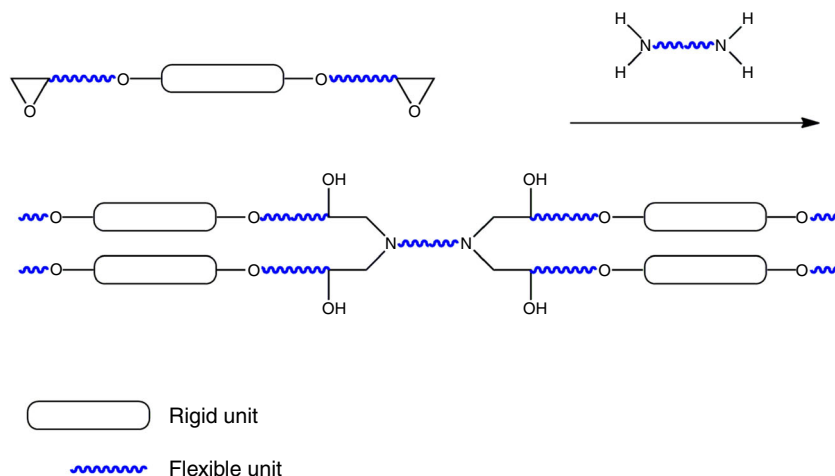
J. Cheng
e-mail: chengjue@mail.buct.edu.cn

Introduction

Epoxy resins possess many outstanding properties such as high mechanical strength and bonding strength, excellent corrosion resistance, good thermal stability, and low shrinkage. As a class of very important thermosetting polymers, epoxy resins have found wide applications in adhesives, protective coatings, electronic encapsulations, advanced composites, etc., [1, 2]. Recently, shape-memory epoxy resins (SMEPs) [3], which are able to temporarily retain a second shape after pre-deformation and recover their 'memorized' permanent shape upon an appropriate stimulus [4–6], are of interest due to the easy tuning [7, 8] of thermal and thermomechanical properties in large range by simply varying the formulations and their excellent shape-memory properties including rapid shape-memory response, high shape fixity, and high shape recovery [9, 10]. However, because of the relatively high crosslink density, traditional epoxy resins often exhibit their brittle nature: their elongation at break is usually low. Thus, enhancement in deformation ability of epoxy resin is desirable to meet the requirement of shape-memory applications. Feldkamp and Rousseau [8, 11] reported that the elongation at break (ε_b) could be improved significantly by simply deforming an SMEP at the onset temperature of the glass transition zone ($T_g^{E'}$). Leonardi et al. [12] prepared an SMEP network with chemical and physical crosslinks and found that this SMEP exhibited relatively high tensile elongation and recovery stress. Recently, we [13, 14] investigated the properties of SMEPs based on intrinsically toughened epoxy resins and found that these SMEPs showed a relatively large elongation around $T_g^{E'}$.

Material design is an effective approach to improve the deformation ability of epoxy network. In this work, a diglycidylether of propoxylated bisphenol-A containing two oxypropylene units (DGEBAPO-2) was prepared, and then

Scheme 1 Chemical structures of DGEBAPO-2 and MPDA

Scheme 2 Network structure of DGEBAPO-2/MPDA system

it was cured by 2-methyl-1,5-pentanediamine (MPDA). The chemical structures of DGEBAPO-2 and MPDA are shown in Scheme 1. DGEBAPO-2 has the characteristic of connecting stiff unit and flexible units together with covalent bonds, and MPDA is a flexible diamine. Thus, an ordered intrinsically toughened network (see Scheme 2) will be formed when DGEABPO-2 is crosslinked with MPDA, and the resultant epoxy system may exhibit relatively large ε_b when performed under proper conditions.

To achieve the desired properties, epoxy systems should be cured into an insoluble and infusible crosslinked network. Since the curing condition may affect the final properties of the cured epoxy resins significantly, it is essential to learn about their curing behaviors. In this aspect, DSC is an effective approach to investigate the curing reaction of epoxy resin systems [15–22]. In our study, non-isothermal and isothermal DSC methods were used to study the curing kinetics of this DGEBAPO-2/MPDA system. Furthermore, the mechanical and thermomechanical properties of the cured epoxy system were investigated by tensile test and DMA, and the shape-memory property of the cured epoxy system was also qualitatively evaluated.

Experimental

Materials

DGEBAPO-2 with epoxide equivalent weight of 233.5 g mol^{-1} was prepared by ourselves, and the curing agent MPDA was obtained from Tianjin Heowns

Biochemical Technology Co., Ltd (Tianjin, China). In present work, DGEBAPO-2 was cured with stoichiometrically equivalent amount of MPDA.

Characterization of DGEBAPO-2

Figure 1 shows the FTIR spectra of propoxylated bisphenol-A containing two oxypropylene units (BAPO-2) and DGEBAPO-2 recorded on a Nicole Nexus 670 FTIR spectrometer in the 4,000–400 cm^{-1} range by using KBr pellets. It can be seen that the broad absorption around 3,365 cm^{-1} (corresponding to the stretching vibration of hydroxyl groups) almost disappears after the epoxidation reaction of BAPO-2 and epichlorohydrin. Moreover, the absorption peak at 907 cm^{-1} assigned to the asymmetrical stretching of epoxy group [23] is observed for DGEBAPO-2, indicating that the epoxy resin is successfully synthesized. ^{1}H NMR experiment was performed on a Bruker Avance 400 spectrometer (400 MHz), using CDCl$_3$ as the solvent, and the ^{1}H NMR spectrum of DGEBAPO-2 with peak assignments is presented in Fig. 2. In particular, $\delta = 3.15$ ppm corresponds to the C$\underline{H}$ of epoxy group (2H), and $\delta = 2.79$ and 2.62 ppm correspond to the C$\underline{H}_2$ of epoxy group (4H) [24, 25]. ESI–MS (Waters Micromass-Quattro Premier XE Mass spectrometer) data: $[M + 18]^+ = 474.4$.

DSC measurements

The non-isothermal cure with varied heating rates of 5, 10, 15, 20, and 25 °C min^{-1} and isothermal cure at different
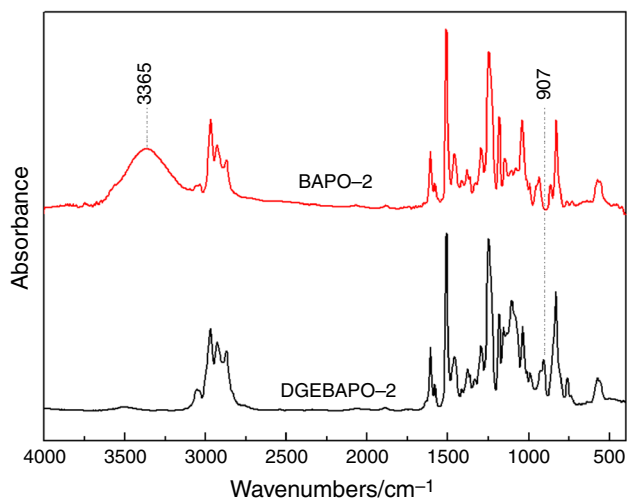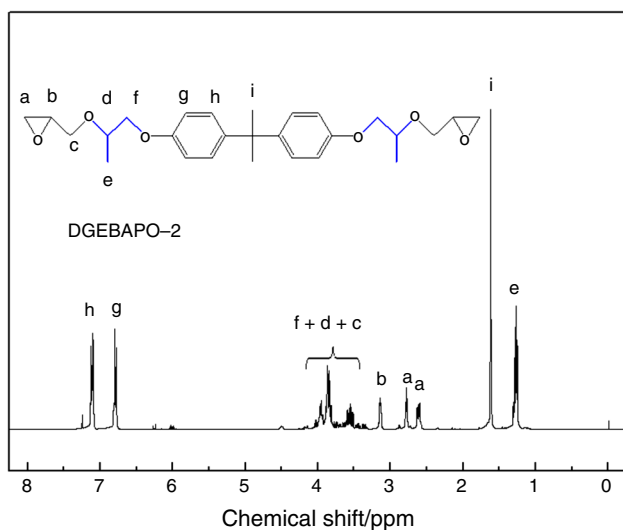
Fig. 1 FTIR spectra of BAPO-2 and DGEBAPO-2

Fig. 2 ^1H NMR spectrum of DGEBAPO-2 in CDCl$_3$

temperatures of 90, 100, 110, 120, and 130 °C were monitored by a TA Instruments Q20 DSC equipped with an RCS 90 cooling system. All the thermal experiments were carried out under the N$_2$ atmosphere. Note here that to start the isothermal experiment, the sample was heated to the isothermal temperature by 90 °C min^{-1}. After the first isothermal run, the sample was cooled to −10 °C, and immediately, a dynamic scan from −10 to 310 °C with 10 °C min^{-1} was performed to determine the residual exothermic heat. Finally, the sample was once again cooled to −10 °C at the maximum cooling rate, followed by a second dynamic run with 10 °C min^{-1} to measure the ultimate glass transition temperature ($T_{g\infty}$) of DGEBAPO-2/MPDA.
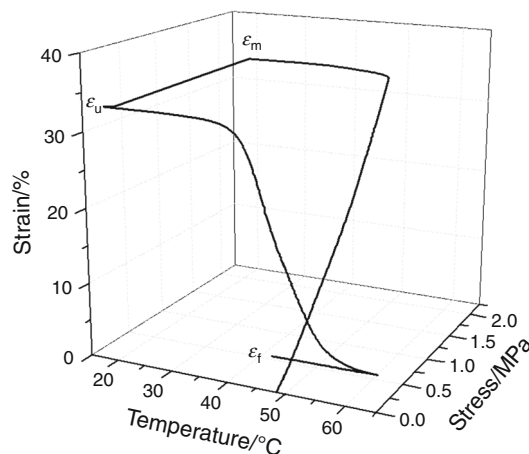

Fig. 3 Typical stress–strain-temperature diagram for quantitative evaluation of shape-memory property

DMA and tensile measurements

For DMA and tensile experiments, DGEBAPO-2 was cured with stoichiometric amount of MPDA at 45 °C for 2 h, 100 °C for 3 h and 130 °C for 4 h. The width of the specimens for DMA measurement is about 3.5 mm, and the thickness is about 0.6–0.7 mm, and the dimensions of the specimens for tensile test met the ASTM D638 requirement (type IV). DMA measurement was carried out on a TA Instruments Q800 DMA at a constant frequency of 1 Hz using the film tension clamps from 0 to 80 °C with a heating rate of 3 °C min^{-1}. The storage modulus, loss modulus, glass transition temperature (T_{gDMA}, defined by the tan δ peaks), and onset temperature of the glass transition zone ($T_g^{E'}$, defined by the intersection temperature of the two tangents to the E'-temperature curve at the glass transition drop) were obtained from the DMA spectrum. Uniaxial tensile test around $T_g^{E'}$ was performed on an Instron 1185 universal tester equipped with a thermostatic chamber. The gage length (l_0) between the clamps was set at 40 mm, and the crosshead speed was fixed at 10 mm min^{-1}. The specimens were equilibrated at the experiment temperature for more than 5 min before programming the tensile test. The value of ε_b can be determined by

$$\varepsilon = \frac{l - l_0}{l_0} \times 100\,\% \tag{1}$$

where ($l - l_0$) is the displacement of the crosshead.

Quantitative evaluation of thermally activated shape-memory property

The shape-memory property of DGEBAPO-2/MPDA was quantitatively characterized by using the Q800 DMA under

the controlled force mode. The procedures were slightly different from those previously reported for the quantitative evaluation of the shape-memory properties [8, 11, 26], and following steps were programmed in present work: the sample was firstly equilibrated at $T_g^{E'}$ for 5 min, and then a force ramp of 1 N min^{-1} was applied, until a stress of about 2 MPa was reached. Secondly, maintained the force applied, the sample was cooled to $T_g^{E'} - 30$ °C with a cooling rate of 3 °C min^{-1}. Thirdly, the force was subsequently released, and then the sample was maintained at $T_g^{E'} - 30$ °C for 5 min. Finally, the sample was reheated to $T_g^{E'} + 20$ °C at a rate of 3 °C min^{-1} and followed by equilibrating at $T_g^{E'}$ for 5 min to start the next shape-memory cycle. Figure 3 shows a typical stress-strain-temperature diagram for one shape-memory cycle and the shape fixity (R_f) and shape recovery (R_r) can be calculated by the following equations:

Shape fixity: $R_f(N) = \dfrac{\varepsilon_u(N)}{\varepsilon_m(N)} \times 100\%$ (2)

Shape recovery: $R_r(N) = \dfrac{\varepsilon_m(N) - \varepsilon_f(N)}{\varepsilon_m(N) - \varepsilon_f(N-1)} \times 100\%$ (3)

where ε_m represents the strain before releasing the force, ε_u represents the fixed strain of the unloaded sample [26] and stabilized at $T_g^{E'} - 30$ °C for 5 min, and ε_f represents the final strain of the sample in the shape-memory cycle.

Results and discussion

Non-isothermal curing reactions of DGEBAPO-2/MPDA

The non-isothermal DSC curves of DGEBAPO-2/MPDA system at the heating rates of 5, 10, 15, 20, and 25 °C min^{-1} are shown in Fig. 4. It can be observed that the peak temperature increases as the heating rate increases; this result is attributed to the fact that at a high heating rate, there is not enough time for curing, and thus the DSC curve will shift to a high temperature to compensate for the reduced time [27]. In the DSC measurement, the reaction exotherms are assumed to be directly proportional to the fractional conversion (α) of the reactive groups; thus, the dependency of α on the temperature can be determined, and the curing reaction rate can be described by Eq. (4) [15, 28].

$$\frac{d\alpha}{dt} = \frac{dH/dt}{\Delta H_0} = k(T)f(\alpha)$$ (4)

where α represents the fractional conversion; t presents the reaction time; dα/dt presents the reaction rate; H presents the reaction exotherm; ΔH_0 presents the total reaction exotherm; $f(\alpha)$ presents the function of α and is associated
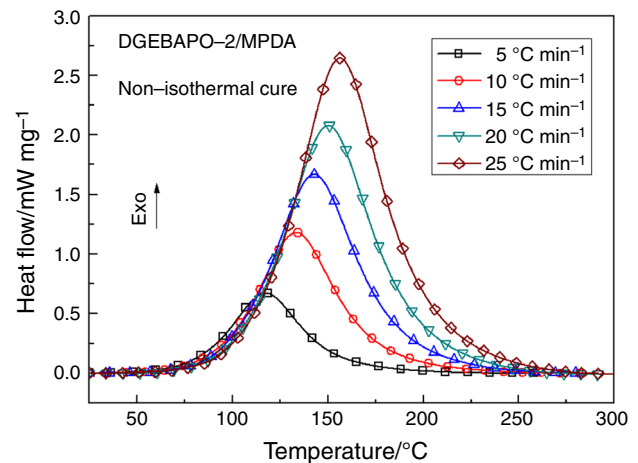

Fig. 4 Non-isothermal DSC curves of DGEBAPO-2/MPDA system at the heating rates of 5, 10, 15, 20 and 25 °C min^{-1}

with the reaction mechanism; $k(T)$ presents the temperature-dependent reaction rate constant and is generally assumed [29] to follow the Arrhenius law:

$$k(T) = A \exp\left(-\frac{E_a}{RT}\right)$$ (5)

where A is the pre-exponential factor; E_a is the apparent activation energy; R is the universal gas constant; T is the absolute temperature.

The kinetic parameter E_α can be calculated by using various methods. In our study, the advanced isoconversional kinetic analysis method [30–32] developed by Vyazovkin was used to reveal the dependency of activation energy on fractional conversion, and then the average activation energy value was obtained. The analytic expressions can be written as

$$\Phi(E_\alpha) = \sum_{i=1}^{n}\sum_{j\neq1}^{n} \frac{J[E_\alpha, T_i(t_\alpha)]}{J[E_\alpha, T_j(t_\alpha)]} = \min$$ (6)

$$J[E_\alpha, T_i(t_\alpha)] \equiv \int_{t_{\alpha-\Delta\alpha}}^{t_\alpha} \exp\left[\frac{-E_\alpha}{RT_i(t)}\right]dt$$ (7)

where the subscripts i and j present the ordinal numbers of the different thermal experiments performed under varied thermal programs, $\Delta\alpha$ presents the small increment of α, and J presents the temperature integral. Note here that the temperature integral was numerically evaluated with a trapezoid rule in the present work.

Figure 5 shows the variation of E_α with α for non-isothermal curing reactions of DGEBAPO-2/MPDA system. It should be pointed out that the ultimate glass transition temperature $T_{g\infty}$ of this DGEBAPO-2/MPDA system was 46.3 ± 0.3 °C; thus, the vitrification was avoided during the non-isothermal cure.

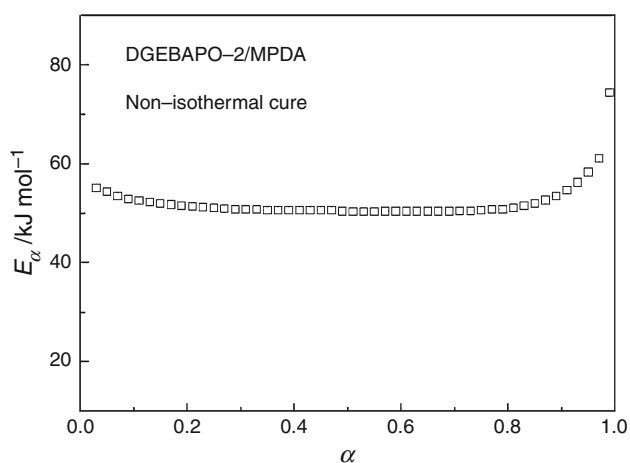**Fig. 5** Variation of E_α with α for non-isothermal curing reactions of DGEBAPO-2/MPDA system

At the beginning of the non-isothermal curing reaction, the value of E_α decreases from 55.1 to about 51 kJ mol^{-1}. This result may be attributed to the decrease in the viscosity [33] of the DGEBAPO-2/MPDA system as the temperature increases gradually. As the non-isothermal curing reaction progresses continuously, the molecular weight increases rapidly; thus, the steric hindrance increases; the increase of steric hindrance will lead to the increase of the activation energy. On the other hand, the secondary hydroxyl groups, which are considered to catalyze the remaining epoxy-amine reaction [17, 34, 35], produce gradually. Thus, the appearance of a plateau stage for $0.21 \leq \alpha \leq 0.81$ with E_α ranging from 50 to 51 kJ mol^{-1} may be due to dynamic compensating balance among the increased molecular weight, elevated temperature, and reinforced autocatalytic effect. When $\alpha > 0.81$, E_α increases rapidly from about 51 to about 74 kJ mol^{-1}, and this result indicates that the rapidly increased molecular weight at the end of the non-isothermal curing reaction may play a more influential role to determine the overall energetic barrier. The average value of the activation energy of DGEBAPO-2/MPDA calculated from the whole E_α–α dependency (see Fig. 5) is 52.2 kJ mol^{-1}.

In order to choose an appropriate kinetic model and further to calculate the kinetic parameters, Málek method [28, 36] was used in our study. According to the Málek method, two special functions $y(\alpha)$ and $z(\alpha)$ can be used to determine a kinetic model and then to estimate the kinetic parameters:

$$y(\alpha) = \left(\frac{d\alpha}{dt}\right)\exp(\chi) \tag{8}$$

$$z(\alpha) = \pi(\chi)\left(\frac{d\alpha}{dt}\right)\frac{t}{\beta} \tag{9}$$

where χ equals to E_α/RT, and $\pi(\chi)$ is the integration of temperature. By a 4th-order rational equation of Senum and

Yang [37], we can calculated the value of $\pi(\chi)$ approximately.

$$\pi(\chi) \approx \frac{\chi^3 + 18\chi^2 + 88\chi + 96}{\chi^4 + 20\chi^3 + 120\chi^2 + 240\chi + 120} \tag{10}$$

According to the experimental data and the average value of the activation energy, we can determine the variation of $d\alpha/dt$, normalized $y(\alpha)$, and normalized $z(\alpha)$ versus α for DGEBAPO-2/MPDA from Málek method. As an example, the variation of $d\alpha/dt$, normalized $y(\alpha)$, and normalized $z(\alpha)$ versus α with the heating rate of 10 °C min^{-1} is shown in Fig. 6. The peak values of da/dt–α, $y(\alpha)$–α and $z(\alpha)$–α curves are, respectively, denoted by α_p, α_M, and α_p^∞, and the results are summarized in Table 1. From this table, we can clearly observe that $0 < \alpha_M < \alpha_p^\infty$ and $\alpha_p^\infty \neq 0.632$; thus, according to the judging standard of the Málek method, the two-parameter Šesták–Berggren model [28, 29, 36], SB(m, n), can be used to fit the non-isothermal curing kinetic of DGEBAPO-2/MPDA system.

The SB(m, n) model can be expressed by the following equation:

$$\frac{d\alpha}{dt} = A\exp(-\chi)\alpha^m(1-\alpha)^n \tag{11}$$

where m and n represent the reaction orders. By logarithmic transformation, Eq. (11) can be transferred to

$$\ln\left[\left(\frac{d\alpha}{dt}\right)\exp(\chi)\right] = \ln A + n\ln\left[\alpha^{m/n}(1-\alpha)\right] \tag{12}$$

where m/n can be replaced by $\alpha_M/(1-\alpha_M)$ [28], and then the kinetic parameters (n, $\ln A$ and m) can be obtained. For instance, the variation of $\ln[(d\alpha/dt)\exp(\chi)]$ versus $\ln[\alpha^{m/n}(1-\alpha)]$ for $0.1 \leq \alpha \leq 0.9$ with the heating rate of 10 °C min^{-1} is shown in Fig. 7. The values of n and $\ln A$ can be, respectively, determined from the slope and intercept of the fitted lines, and then the value of m can be obtained by multiplying n and $\alpha_M/(1-\alpha_M)$ together. These results for varied heating rates are also presented in Table 1.

Substitution of the calculated kinetic parameters into Eq. (11) yields an explicit rate equation for predicting the non-isothermal curing reaction of DGEBAPO-2/MPDA system:

$$\frac{d\alpha}{dt} = 3.942 \times 10^6 \exp\left(\frac{-52200}{RT}\right)\alpha^{0.493}(1-\alpha)^{1.752} \tag{13}$$

In the present work, an ordinary differential equation solver program based on the 4th-order Runge–Kutta Method was used to simulate the model predicted curves. Note here that the initial condition for solving Eq. (13) was set as $\alpha = 0.005$ when $T = 273.15$ K. The model-simulated curves and the experimental curves are compared in Fig. 8; furthermore, the values of peak reacting rate

Fig. 6 Plots of (dα/dt), normalized $y(\alpha)$, and normalized $z(\alpha)$ versus α for DGEBAPO-2/MPDA system with the heating rate of 10 °C min^{-1}
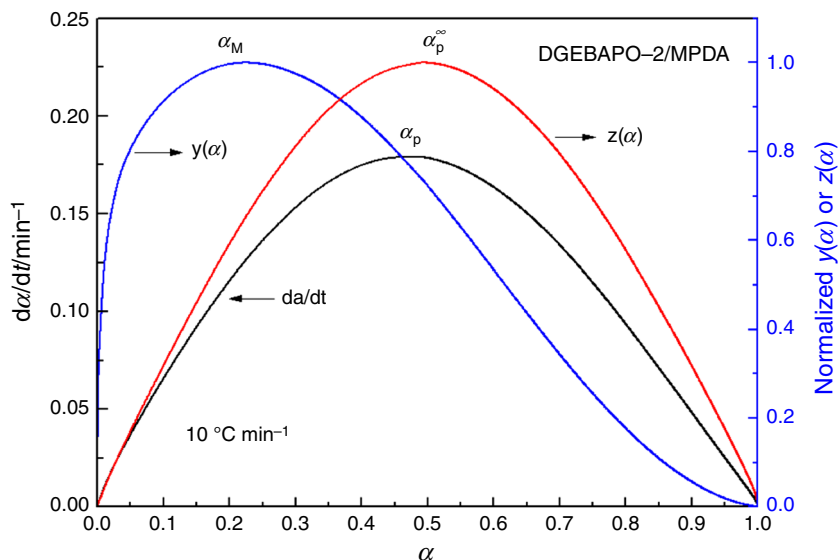

Table 1 The peak values of dα/dt, $y(\alpha)$, and $z(\alpha)$, along with the calculated kinetic parameters (n, m and ln$A$) for non-isothermal cure of DGEBAPO-2/MPDA system with different heating rates

Heating rate/°C min^{-1}	α_p	α_M	α_p^∞	n	m	ln$A$
5	0.488	0.232	0.504	0.544	1.804	15.296
10	0.483	0.226	0.494	0.516	1.771	15.220
15	0.476	0.212	0.491	0.462	1.720	15.142
20	0.471	0.209	0.492	0.454	1.724	15.116
25	0.473	0.219	0.497	0.488	1.740	15.163
Mean				0.493	1.752	15.187

Fig. 8 Comparison of experimental rates (*dots*) and simulated rates (*full lines*) for the non-isothermal curing reaction of DGEBAPO-2/MPDA system with different heating rates

heating rates are summarized in Table 2. From Fig. 8 and Table 2, we may draw a conclusion that Eq. (13) can appropriately describe the non-isothermal reaction of DGEBAPO-2/MPDA system.

Isothermal curing reactions of DGEBAPO-2/MPDA

The isothermal DSC curves of DGEBAPO-2/MPDA system at five different temperatures are shown in Fig. 9. From this figure, one can observe that a main exothermic peak of the curing reaction appears at $t > 0$; thus, the autocatalytic Kamal model [38], as shown in Eq. (14), may be used to describe the isothermal curing reaction of DGEBAPO-2/MPDA system.
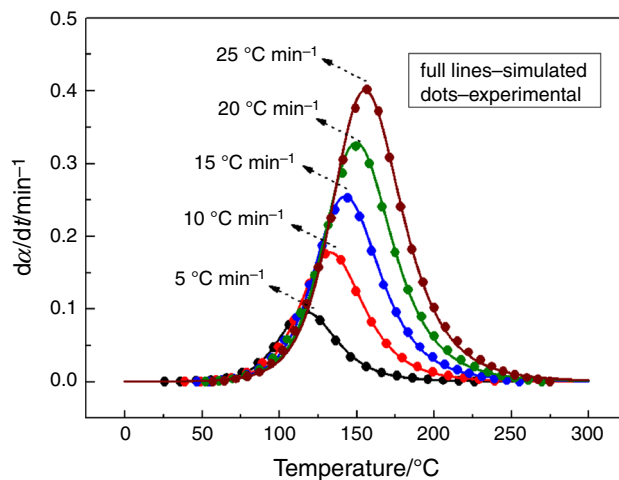

Fig. 7 Variation of [(dα/dt) exp (χ)] versus ln [$\alpha^{m/n}(1 - \alpha)$] for DGEBAPO-2/MPDA with the heating rate of 10 °C min^{-1}

(dα/dt)$_p$ together with the corresponding conversion fraction (α_p) and temperature (T_p) were determined from the experimental curves, and the simulated curves at different

Table 2 The peak values of dα/dt together with the corresponding α_p and T_p determined from experimental curves and SB(m, n) model at different heating rates

Heating rate/°C min⁻¹	Experimental data			Calculated data from SB(m, n) model		
	T_p/°C	α_p	Peak value of dα/dt/min⁻¹	T_p/°C	α_p	Peak value of dα/dt/min⁻¹
5	118.4	0.488	0.098	117.4	0.458	0.096
10	134.3	0.483	0.179	132.9	0.456	0.177
15	143.3	0.476	0.253	142.6	0.456	0.254
20	150.4	0.471	0.323	149.7	0.456	0.329
25	156.5	0.473	0.402	155.4	0.455	0.400

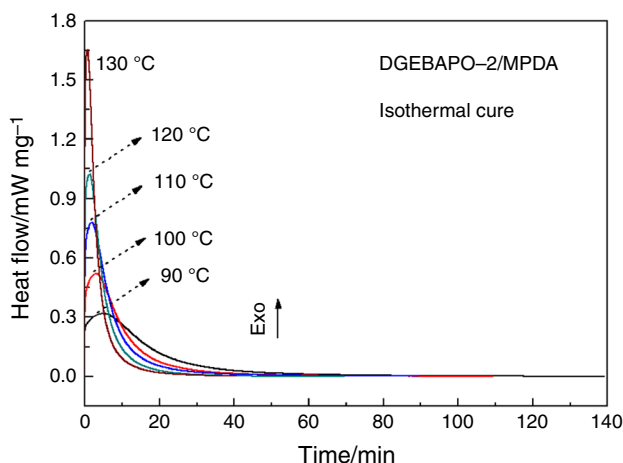The initial condition is set as $\alpha = 0.005$ when $T = 273.15$ K

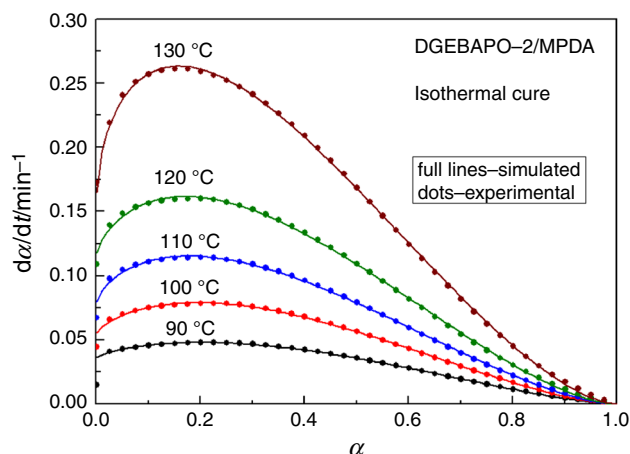**Fig. 9** Isothermal DSC curves of DGEBAPO-2/MPDA system at different temperatures

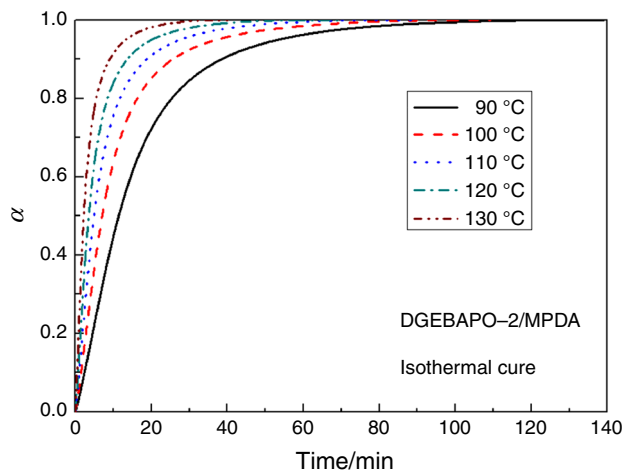**Fig. 11** Comparison of experimental data and simulated data for DGEBAPO-2/MPDA system at different temperatures

Fig. 10 Relationship between α and time at different temperatures

$$\frac{d\alpha}{dt} = (k_1 + k_2\alpha^{m_k})(1 - \alpha)^{n_k} \qquad (14)$$

where k_1 represents the non-autocatalyzed rate constant, k_2 represents the autocatalyzed rate constant, and m_k and n_k are the reaction orders. The relationship between the absolute curing degree and time can be determined by

$$\alpha_{absolute} = \frac{\Delta H_t}{\Delta H_{iso} + \Delta H_{res}} \qquad (15)$$

where ΔH_t represents the cumulative heat at time t, ΔH_{iso} represents the isothermal reaction heat, and ΔH_{res} represents the residual reaction heat. It should be pointed out that in our study, the curing reaction temperatures are well above $T_{g\infty}$ of DGEBAPO-2/MPDA system and ΔH_{res} (< 3 J g⁻¹) $\ll \Delta H_{iso}$; thus, the values of absolute curing degree and relative curing degree are numerically indistinguishable. Thus, relative curing degree was used, and the relationship between α and time at different temperatures is presented in Fig. 10.

Figure 11 displays the variation of dα/dt versus α at different temperatures. By a nonlinear least-square fitting procedure, we can obtain the isothermal kinetic parameters

for the Kamal model. The results are summarized in Table 3, and the simulated plots are also shown in Fig. 11. From Table 3, we can observe that k_2 is much greater than k_1, indicating that the rate of autocatalytic reaction is greater than that of non-autocatalytic reaction. As shown in

Table 3 Kinetic parameters of Kamal model for isothermal cure of DGEBAPO-2/D230 system

Temperature/°C	k_1/min^{-1}	k_2/min^{-1}	m_k	n_k
90	0.036	0.119	0.832	1.527
100	0.055	0.198	0.757	1.600
110	0.078	0.265	0.687	1.618
120	0.115	0.368	0.713	1.638
130	0.154	0.533	0.546	1.625
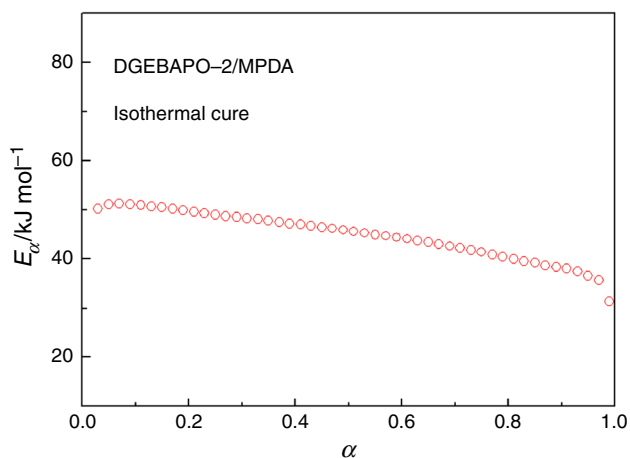
Fig. 12 E_α-α dependency for isothermal curing reactions of DGEBAPO-2/MPDA system
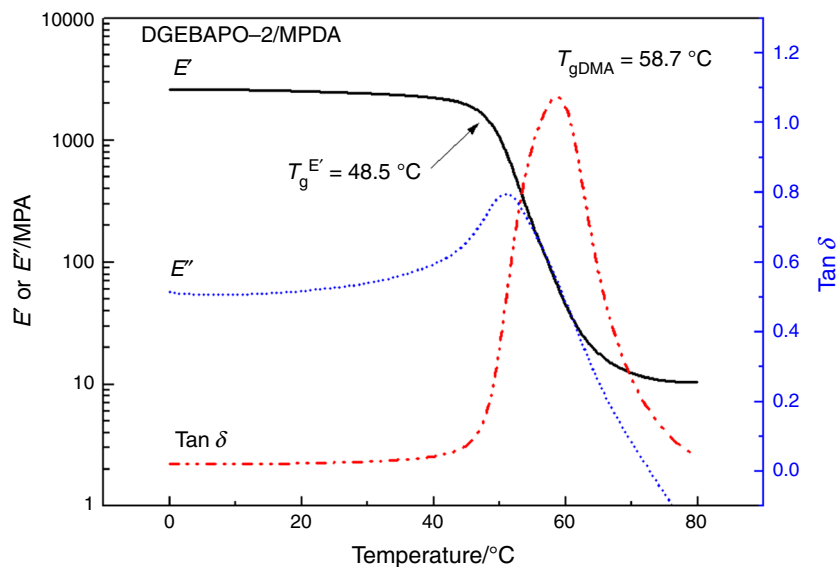
Fig. 11, the calculated data are in good agreement with the experimental results.

Using the advanced isoconversional kinetic analysis method developed by Vyazovkin, we can also determine the E_α-α dependency of the isothermal curing reaction of DGEBAPO-2/MPDA. As shown in Fig. 12, the isothermal E_α-α dependency is quite different from the corresponding non-isothermal E_α-α dependency, indicating that the curing reaction is very complex. Note here that the isothermal reaction temperatures are all much higher than $T_{g\infty}$ of the cured epoxy resin; thus, the vitrification of the epoxy resin system is avoided, and the vitrification-induced diffusion-controlled cure will not occur during the isothermal cure. As α increases, E_α of isothermal cure decreases gradually. The decrease in E_α may be associated with the increase in hydroxyl groups formed during the curing reaction of DGEBAPO-2/MPDA [17, 34, 35].

Dynamic mechanical and mechanical properties

The DMA curves of the cured DGEBAPO-2/MPDA system are displayed in Fig. 13. The storage modulus depends heavily on temperature: with rising of temperature, a large and sharp drop of storage modulus in the glass-to-rubber transition zone can be observed. The E' in glass state is over 2 orders of magnitude larger than E' in rubber state, suggesting that the cured epoxy resin may possess good shape-memory performance. $T_g^{E'}$ of the cured DGEBAPO-2/MPDA is 48.5 °C, according to the DMA, and tensile experiment was performed around $T_g^{E'}$ (in our study, the temperature for tensile test was set at 49 °C). A combination of relatively large tensile stress (6.33 ± 0.11 MPa) and elongation at break (95.53 ± 2.27 %), which may be

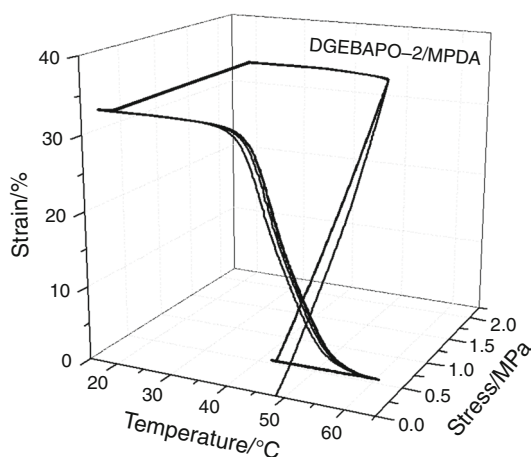**Fig. 13** DMA curves of the cured DGEBAPO-2/MPDA system

Fig. 14 Consecutive shape-memory cycles for cured DGEBAPO-2/MPDA system

necessary for shape-memory applications, can be observed from the tensile experiment.

Shape-memory properties

Figure 14 shows the stress–strain-temperature diagram for consecutive shape-memory cycles of cured DGEBAPO-2/MPDA. A close inspection of the three-dimensional diagram reveals that the first shape-memory cycle is a little different from the subsequent curves. This difference may be caused by the plastic deformation arising from molecular rearrangement of the network chains [11]. The values of R_f and R_r during four consecutive shape-memory cycles are, respectively, 98.88 ± 0.04 and 96.67 ± 6.91 %, indicating good shape fixity and shape recovery of DGEBAPO-2/MPDA system.

Conclusions

An intrinsically toughened network for potential shape-memory application was prepared by curing DGEBAPO-2 and MPDA. The non-isothermal and isothermal curing kinetics of DGEBAPO-2/MPDA were systematically investigated by DSC, and the thermal mechanical property, mechanical property, and shape-memory property of the cured material were characterized by DMA, tensile tester, and quantitative shape-memory evaluation method. The curing reaction studies indicated that Šesták-Berggren model and Kamal model were able to, respectively, stimulate the non-isothermal curing reaction rate and isothermal curing reaction rate. The E_α–α dependencies between non-isothermal cure and isothermal cure were different, indicating complex curing kinetics of DGEBAPO-2/MPDA. The DMA disclosed that this SMEP showed a large variation (more than 2 orders of magnitude) in E' during its glass transition. $T_g^{E'}$ of the SMEP was 48.5 °C, and the tensile experiment around $T_g^{E'}$ showed that this SMEP exhibited a combination of relatively large elongation at break (95.53 ± 2.27 %) and tensile stress (6.33 ± 0.11 MPa). Quantitative shape-memory evaluation revealed that this SMEP possessed good shape-memory properties with shape fixity of 98.88 ± 0.04 % and shape recovery of 96.67 ± 6.91 %.

References

1. Pascault JP, Williams R. Epoxy polymers: new materials and innovations. Weinheim: Wiley-VCH; 2010.
2. Petrie EM. Epoxy adhesive formulations. New York: McGraw-Hill Professional; 2006.
3. Santhosh Kumar KS, Biju R, Reghunadhan Nair CP. Progress in shape memory epoxy resins. React Funct Polym. 2013;73(2):421–30.
4. Hu J, Institute T. Shape memory polymers and textiles. Cambridge: Woodhead Publishing Limited; 2007.
5. Lendlein A. Shape-memory polymers. Heidelberg: Springer-Verlag; 2010.
6. Rousseau IA, Xie T. Shape memory epoxy: composition, structure, properties and shape memory performances. J Mater Chem. 2010;20(17):3431–41.
7. Xie T, Rousseau IA. Facile tailoring of thermal transition temperatures of epoxy shape memory polymers. Polymer. 2009;50(8):1852–6.
8. Feldkamp DM, Rousseau IA. Effect of chemical composition on the deformability of shape-memory epoxies. Macromol Mater Eng. 2011;296(12):1128–41.
9. Liu Y, Han C, Tan H, Du X. Thermal, mechanical and shape memory properties of shape memory epoxy resin. Mater Sci Eng, A. 2010;527(10):2510–4.
10. Wei K, Zhu G, Tang Y, Tian G, Xie J. Thermomechanical properties of shape-memory hydro-epoxy resin. Smart Mater Struct. 2012;21(5):55022.
11. Feldkamp DM, Rousseau IA. Effect of the deformation temperature on the shape-memory behavior of epoxy networks. Macromol Mater Eng. 2010;295(8):726–34.
12. Leonardi AB, Fasce LA, Zucchi IA, Hoppe CE, Soulé ER, Pérez CJ, Williams RJ. Shape memory epoxies based on networks with chemical and physical crosslinks. Eur Polym J. 2011;47(3):362–9.
13. Fan M, Yu H, Li X, Cheng J, Zhang J. Thermomechanical and shape-memory properties of epoxy-based shape-memory polymer using diglycidyl ether of ethoxylated bisphenol-A. Smart Mater Struct. 2013;22(5):55034.
14. Fan M, Liu J, Li X, Zhang J, Cheng J. Thermal, mechanical and shape memory properties of an intrinsically toughened epoxy/anhydride system. J Polym Res. 2014;21:376.
15. Sbirrazzuoli N, Vyazovkin S. Learning about epoxy cure mechanisms from isoconversional analysis of DSC data. Thermochim Acta. 2002;388(1):289–98.
16. Macan J, Brnardić I, Ivanković M, Mencer HJ. DSC study of cure kinetics of DGEBA-based epoxy resin with poly (oxypropylene) diamine. J Therm Anal Calorim. 2005;81(2):369–73.

17. Wan J, Bu Z, Xu C, Li B, Fan H. Learning about novel amine-adduct curing agents for epoxy resins: butyl-glycidylether-modified poly (propyleneimine) dendrimers. Thermochim Acta. 2011;519(1):72–82.

18. Wan J, Fan H, Li B, Xu C, Bu Z. Synthesis and nonisothermal reaction of a novel acrylonitrile-capped poly (propyleneimine) dendrimer with epoxy resin. J Therm Anal Calorim. 2011;103(2):685–92.

19. Wang H, Zhang Y, Zhu L, Zhang B, Zhang Y. Curing behavior and kinetics of epoxy resins cured with liquid crystalline curing agent. J Therm Anal Calorim. 2012;107(3):1205–11.

20. Wan J, Li C, Bu Z, Xu C, Li B, Fan H. A comparative study of epoxy resin cured with a linear diamine and a branched polyamine. Chem Eng J. 2012;188:160–72.

21. Saad GR, Naguib HF, Elmenyawy SA. Effect of organically modified montmorillonite filler on the dynamic cure kinetics, thermal stability, and mechanical properties of brominated epoxy/aniline formaldehyde condensates system. J Therm Anal Calorim. 2013;111(2):1409–17.

22. Li C, Liu M, Liu Z, Qing M, Wang G. DSC and curing kinetics of epoxy resin using cyclohexanediol diglycidyl ether as active diluents. J Therm Anal Calorim. 2014;116(1):411–6.

23. Lee K, Kim J, Bae J, Yang J, Hong S, Kim H. Studies on the thermal stabilization enhancement of ABS; synergistic effect by triphenyl phosphate and epoxy resin mixtures. Polymer. 2002;43(8):2249–53.

24. Herrera González AM, D'Accorso NB, Cuevas Suárez CE, Fascio ML, García Serrano J, Alho MM, Zamarripa Calderón JE. Composite resins based on novel and highly reactive bisglycidyl methacrylate monomers. J Appl Polym Sci. 2014.

25. Fan M, Liu J, Li X, Cheng J, Zhang J. Curing behaviors and properties of an extrinsic toughened epoxy/anhydride system and an intrinsic toughened epoxy/anhydride system. Thermochim Acta. 2013;554:39–47.

26. Saralegi A, Foster EJ, Weder C, Eceiza A, Corcuera MA. Thermoplastic shape-memory polyurethanes based on natural oils. Smart Mater Struct. 2014;23(2):25033.

27. Zhao SF, Zhang GP, Sun R, Wong CP. Curing kinetics, mechanism and chemorheological behavior of methanol etherified amino/novolac epoxy systems. Express Polym Lett. 2014;8(2).

28. Málek J. The kinetic analysis of non-isothermal data. Thermochim Acta. 1992;200:257–69.

29. Šesták J, Berggren G. Study of the kinetics of the mechanism of solid-state reactions at increasing temperatures. Thermochim Acta. 1971;3(1):1–12.

30. Vyazovkin S. Advanced isoconversional method. J Therm Anal Calorim. 1997;49(3):1493–9.

31. Vyazovkin S. Evaluation of activation energy of thermally stimulated solid-state reactions under arbitrary variation of temperature. J Comput Chem. 1997;18(3):393–402.

32. Vyazovkin S. Modification of the integral isoconversional method to account for variation in the activation energy. J Comput Chem. 2001;22(2):178–83.

33. Vyazovkin S, Sbirrazzuoli N. Effect of viscosity on the kinetics of initial cure stages. Macromol Chem Phys. 2000;201(2):199–203.

34. Smith IT. The mechanism of the crosslinking of epoxide resins by amines. Polymer. 1961;2:95–108.

35. Xu L, Fu JH, Schlup JR. In situ near-infrared spectroscopic investigation of epoxy resin-aromatic amine cure mechanisms. J Am Chem Soc. 1994;116(7):2821–6.

36. Málek J. A computer program for kinetic analysis of non-isothermal thermoanalytical data. Thermochim Acta. 1989;138(2):337–46.

37. Senum GI, Yang RT. Rational approximations of the integral of the Arrhenius function. J Thermal Anal. 1977;11(3):445–7.

38. Kamal MR. Thermoset characterization for moldability analysis. Polym Eng Sci. 1974;14(3):231–9.